Asian Journal of Chemistry; Vol. 33, No. 1 (2021), 203-209

ASIAN JOURNAL OF CHEMISTRY

https://doi.org/10.14233/ajchem.2021.22983

Mechanical, Thermal Properties and Hirshfeld Surface Analysis of *N*-Acetylglycine Single Crystal

V.J. THANIGAIARASU[1], N. KANAGATHARA[2,*], R. USHA[2], V. SABARI[3] and V. NATARAJAN[4]

[1]Department of Physics, Jaya College of Arts and Science, Thiruninravur-602024, India
[2]Department of Physics, Saveetha School of Engineering, Saveetha Institute of Medical and Technical Sciences, Thandalam-602105, India
[3]Department of Physics, Marudhar Kesari Jain College for Women, Vaniyambadi-635751, India
[4]Department of Physics, Rajalakshmi Institute of Technology, Kuthambakkam-602124, India

*Corresponding author: E-mail: kanagathara23275@gmail.com

Received: 5 September 2020; *Accepted*: 30 October 2020; *Published online*: 10 December 2020; AJC-20199

Mechanical properties of some amino acid based derivatives plays a versatile role in the device fabrication due to its mechanical strength. One such acetyl derivative of glycine named *N*-acetylglycine has been taken in the present study for investigation. Hardness analysis has been carried out on the grown crystal with various loads and it was observed that Vicker's hardness number (Hv) varied for different loads. The work hardening coefficient is calculated to be 1.628 which confirms that the grown crystal comes under moderately hard material category. Other mechanical parameters like minimum load indentation (W), materials constant (k_1), load dependent constant (A_1) and elastic stiffness constant (C_{11}) have also been calculated. The thermal analysis has also been carried and it reveals that the complete weight loss of *N*-acetylglycine starts from 208.60 ºC and ends at 281.58 ºC. The corresponding DTA peak is observed at 217.97 ºC which is the melting point of the sample. As expected, there is no phase transition till the material melts and this enhances the temperature range for the utility of the crystal. Kinetic and thermodynamic parameters have been calculated. All the results obtained from hardness as well as thermal measurement confirm the material may be suitable for electro-optic device applications. Further, the 3D Hirshfeld surface analysis and 2D fingerprint maps gives deep insight into the intermolecular interactions between the compound.

Keywords: *N*-Acetylglycine, Elastic stiffness constant, Meyer's index, Vicker's Hardness number, Hirshfeld.

INTRODUCTION

The science of the advanced materials needs true prediction of material behaviour before application. No crystal is either too soft or too hard to prevent the determination of its elastic, plastic and cracking properties under a suitable probing indenter. A sampling of the wealth of measurements and reported analyses associated with the topic on a wide variety of materials are presented in the current special issue. Importance of hardness with material compaction in softer organic crystals relates to pharmaceutical tableting [1] and formulated energetic material processing applications [2]. Structural, vibrational, dielectric and ferroelectric properties of *N*-acetylglycine have been extensively studied by various researchers [3-10]. The single crystal XRD data of *N*-acetylglycine crystal indicates that it crystallizes in the monoclinic system with centro symmetric space group $P2_1/c$ with lattice a = 4.8410(10) Å, b = 11.512(2) Å, c = 9.810(2) Å, $\alpha = 90°$, $\beta = 97.02(3)°$, $\gamma = 90°$ and V = 542.61 $(Å)^3$. Materials with high optical intensities and good mechanical strength possess non-linear optical behaviour. Such materials get degraded when electric field or mechanical stress is applied on it. Hence it is necessary to test the strength as well as deformation characteristics of the material by Vicker's hardness method before application. Several researchers [11-17] reported the mechanical properties of few complexes of glycine with zinc chloride, lithium sulphate, triglycine sulphate and phosphoric acid. In this communication, mechanical parameters are calculated to identify the strength of the grown crystal. In addition to that, the thermal stability of the grown crystal is determined by thermogravimetric (TG) analysis based on the measurement of mass loss of material as a function of temperature. TGA has also been used to elucidate the kinetics of decomposition reactions by analyzing the shape of the thermal curve. In general, the rate of reaction at any measured temperature is proportional to the slope of the curve, but a number of uncertainties some-times make this analysis of questionable

value. Both isothermal and dynamic methods are in use of kinetic studies but the iso-thermal measurement at elevated temperature is easy and the time taken for the measurement of certain extent of mass loss to occur is simpler. According to the International Confederation for Thermal Analysis and Calorimetry (ICTAC), multiple heating rate programs should be used for computation of reliable kinetic parameters [18-20]. Either single heating methods like Broido, Horowitz-Metzger, Freeman-Caroll, Chang and Coats-Redfern or multiple heating methods like Flynn-Wall, Friedman, Kim-Park, Kissinger and Hernandez-Sanchez methods are used to investigate the kinetic parameters of the given material [21,22]. In the present study thermal decomposition kinetics and thermodynamic properties are calculated by single heating rate methods *viz.* Broido, Horowitz-Metzger and Coats-Redfern methods. Also Hirshfeld surface analysis and first order hyper polarizability calculations has been done for the grown *N*-acetylglycine single crystal and discussed in detail.

EXPERIMENTAL

Crystals of *N*-acetylglycine [$C_4H_7NO_3$] were obtained by crystallization at room temperature from an aqueous solution containing AR grade samples of *N*-acetylglycine by the slow evaporation process and the pH value is measured as 1. During a few days, tiny colourless crystals were produced. The photograph of the crystal is shown in Fig. 1.

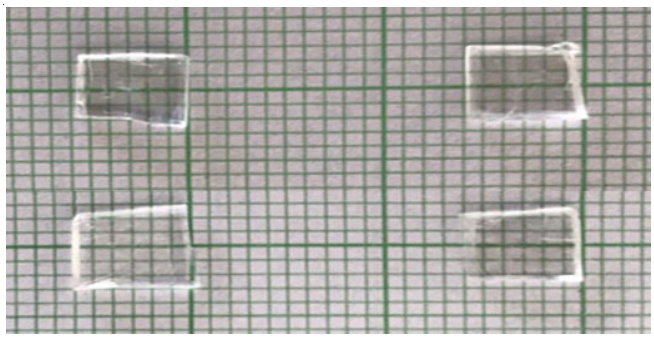

Fig. 1. Photograph of as-grown crystal of *N*-acetylglycine

Characterization: The grown crystals of *N*-acetylglycine was exposed to single crystal XRD analysis using KUMA KM-4 single crystal X-ray diffractometer geared up with a two-dimensional area CCD detector with M_oK_α (λ = 0.71073 Å) radiation. Hardness measurement has been carried out on the grown crystal with various loads by using Economet (Model VH1MD) hardness tester, with Vicker's pyramidal diamond indenter. The thermogravimetric analysis of pure *N*-acetylglycine was carried out using Perkin Elmer simultaneous Thermal analyser STA 6000 between 0-800 °C at a heating rate of 10 °C/min with nitrogen atmosphere.

RESULTS AND DISCUSSION

Single crystal X-ray diffraction analysis: The single crystal XRD analysis of *N*-acetylglycine indicates that it crystallizes in the monoclinic system with centro symmetric space group $P2_1/c$ with lattice a = 4.8410 (10) Å, b = 11.512(2) Å, c = 9.810(2) Å, $\alpha = 90°$, $\beta = 97.02(3)°$, $\gamma = 90°$ and V = 542.61 $(Å)^3$.

Mechanical studies of pure *N*-acetylglycine: Hardness of a material is the measure of resistance when it offers to local deformation. The mechanical properties like hardness number, Meyer's index, yield strength and elastic stiffness constant are important parameters in device fabrication and are used to analyse the mechanical strength of the material [23]. The crystal of good quality in size is taken for hardness measurement. The loads ranging from 10 to 100 g were used for hardness studies and the loads were applied slowly by pressing the indenter on the surface of the sample being tested. The average value of indentation impression for every load was used to calculate Vicker's microhardness value (H_v).

$$H_v = \frac{1.8544p}{d2}(kg/mm^2) \quad (1)$$

where p is the applied load and d is the diagonal length of indentation in mm.

Fig. 2 depicts the variation of load with Vicker's hardness number. From the figure it is observed that hardness decreases with increase in load which is the normal reverse indentation size effect [24]. Beyond 200 g there is a crack in the material. Meyer's law gives the relation between the variation in load (P) and indentation (d). The value of material constant is calculated from the slope of the straight line. Fig. 3 depicts the variation of d^n with load P. According to Meyer's law, the relation connecting the applied load is given by:

$$P = k_1 d^n \quad (2)$$

$$\log P = \log k + n \log d \quad (3)$$

where n is the Meyer index or work hardening exponent and k_1, is the constant for a given material. The above relation indicates that 'H_v' should increase with load P if n > 2 and decrease with load P when n < 2. The value of work hardening coefficient determines the effect of dislocation in the crystal. The less value of work hardening coefficient inculcate the less defect in the crystal [25-27]. The plot of log d *vs.* log P (Fig. 4) gives work hardening coefficient (n) as 1.628. Materials that possess work hardening coefficient in between 1-1.6 come under moderately hard material [28-31]. The moderate hardness value suggests that the material may be useful for

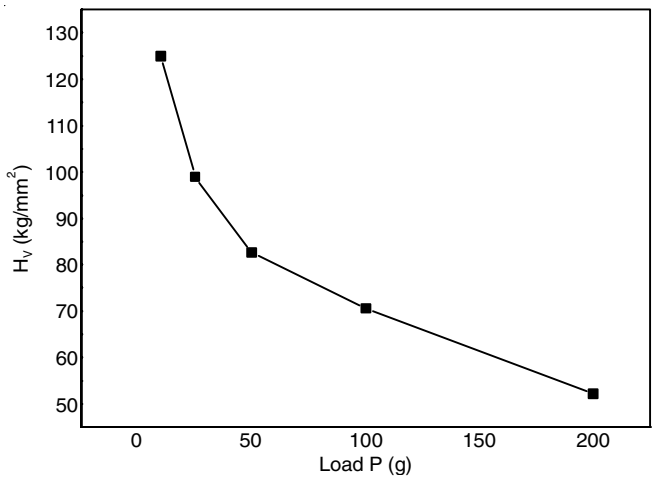

Fig. 2. Load P (g) *vs.* Vicker's hardness (H_v) (kg/mm^2)

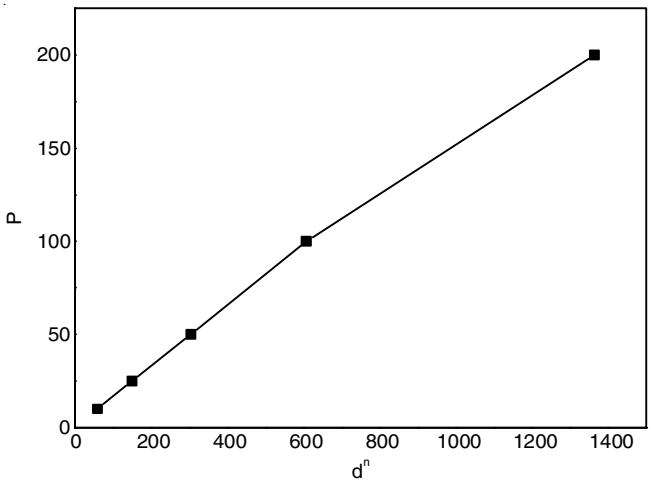

Fig. 3. Plot of d^n *vs*. P

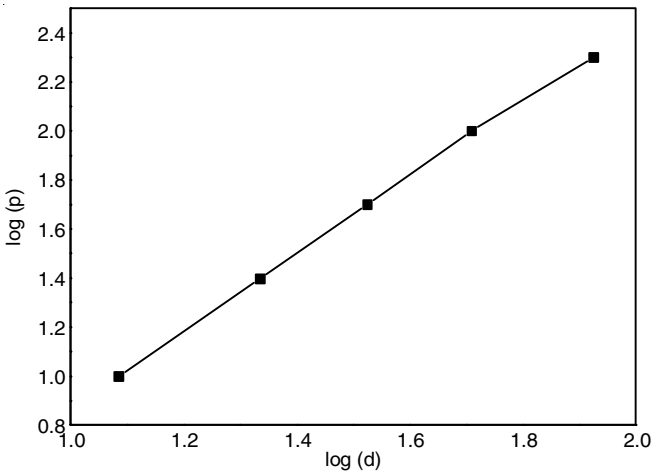

Fig. 4. Plot of log d *vs*. log P

pharmaceutical tableting and energetic material processing applications. The elastic stiffness constant is calculated to be 2.346 by the Wooster's empirical relation $C_{11}=H_v^{7/4}$. This high value gives the strength of the bond in the grown crystal [31]. The values obtained are almost similar to the reported values of glycine complexes [27-30].

Thermal analysis of pure *N*-acetylglycine: It is well known that the thermal treatment is needed for the protein containing food stuffs in amino acids formed in the course of hydrolysis are subject to temperature. In present study, the thermal decomposition of *N*-acetylglycine and establishes the formation of composition of products. The TG curve exhibits mass losses in a single stage which indicates that decomposition of the grown crystals takes place sharply (Fig. 5). Initial mass is taken as 5.472 mg. The sharpness of the endo or exothermic peak shows good degree of crystallinity of the grown sample. The absence of water of crystallization in the molecular structure of *N*-acetylglycine is indicated by the absence of the weight loss around 100 ºC. Thermal curve reveals that complete weight loss of *N*-acetylglycineght starts from 208.60 ºC and ends at 281.58 ºC. The corresponding DTA peak is observed at 214.97 °C which is the melting point of the sample. The decomposition ends with a final residue of 0.6952 mg. Glycine melting range varies

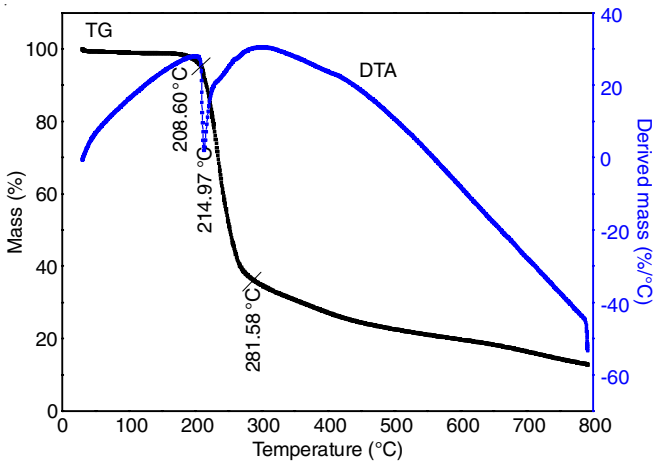

Fig. 5. TG-DTA of *N*-acetylglycine crystal

from 232-236 °C [32,33]. Comparative study of the thermal decomposition behaviour of different amino acids and peptides was reported by Schaberg *et al.* [34]. As expected, it is clear that the thermal stability of *N*-acetylglycine is more and there is no phase transition till the material melts and this enhances the temperature range for the utility of the crystal for applications. Under these conditions, phase transition means common phase transition like solid to liquid or liquid to gas, *etc*.

Kinetic and thermodynamic parameters: Thermogravimetric and differential thermal analysis (TG-DTA) – an analytical technique is acceptable by many researchers and attempts have been made to calculate various thermodynamic parameters during thermal degradation which important for the applications of thermal analysis [35]. Solid state kinetics is extensively studied by thermal analysis method.

TGA kinetics analysis is determined by measurement of fractional mass loss and degradation rate according to temperature change. In the present study, Kinetic parameters are evaluated from TG-DTA data by single heating method like Broido, Coats-Redfern and Horowitz-Metzger method [36].

TGA kinetics analysis is determined by the measurement of fractional mass loss and degradation rate according to temperature change. The fraction of conversion (α), is defined as:

$$\alpha = \left(\frac{W_o - W}{W_o - W_f} \right) \tag{4}$$

where, W is the actual mass at any degradation time, W_o is the initial mass and W_f is the final mass at the end of the thermal degradation process. The rate of degradation (dα/dt) can be expressed as the product of the function of temperature and the function of conversion:

$$\frac{d\alpha}{dt} = \beta \frac{d\alpha}{dt} = k(T).f(\alpha) \tag{5}$$

where β = dT/dt is the heating rate.

For non-isothermal experiment, the reaction rate at all times depends on both f(α) and k(T). Hence, generally f(α), k(T) and ln A are known as kinetic triplet.

Arrehenius temperature dependent function is given by

$$\ln k = \ln A - \frac{E_a}{RT} \tag{6}$$

where E_a is the activation energy, A is a pre-exponential factor and R is the gas constant.

The linear Arrhenius plots of ln k *versus* 1000/T can be plotted from the non-isothermal TG data. The slope of the linear plot gives the activation energy which is found to be 122.04 KJ mol^{-1}. Yablokov *et al*. [33] reported the activation energy value of glycine as 157 KJ mol^{-1} and the melting point as 262 °C based on Arrhenius plot.

The other thermodynamical parameters like entropy, enthalpy and Gibb's free energy can be calculated [37]. The standard entropy of activation is calculated from the expression:

$$\Delta S = 2.303 \times R \times \log_{10}\left(\frac{Ah}{kT_m}\right) \quad (7)$$

where, k = Boltzmann constant, h = Planck's constant, T_m = temperature, A = frequency factor. It is found to be 197.73 JK^{-1} mol^{-1}.

The standard enthalpy of activation (ΔH) can be calculated be 113.95 JK^{-1} mol^{-1} by using the following relation:

$$\Delta H = E\text{-}2RT \quad (8)$$

The standard Gibbs energy of activation (ΔG) is possible to estimate from the equation:

$$\Delta G = \Delta H - T\Delta S \quad (9)$$

and it is found to be 17.66 JK^{-1} mol^{-1}.

Broido method [38]**:** Broido's method of calculation of activation energy is obtained from following expression:

$$\ln\left(\ln\frac{1}{\alpha}\right) = \frac{-E_a}{RT} + \frac{RAT^2}{E_a\beta} \quad (10)$$

The value of the activation energy (E_a) can be calculated from the slope of the plot of graph between ln [ln(1/α)] and 1/T. The calculated activation energy is 76.97 KJ mol^{-1}.

Horowitz-Metzger method [39]**:** The activation energy is calculated by Horowitz-Metzger method from following expression:

$$\ln\ (1-\alpha) = \frac{E_a(T-T_p)}{RT_p} \quad \text{for n=1} \quad (11)$$

The slope of the plot of graph between ln (1-α) and 1/T gives the activation energy (E_a). The calculated activation energy is 39.91 KJ mol^{-1}.

Coats-Redfern method [40]**:** Coats-Redfern relation is given as:

$$\ln\left(-\ln\frac{1-\alpha}{T^2}\right) = \ln\left(\frac{AR}{\beta E_a}\right)\left(\frac{1-2RT}{E_a}\right) - \frac{E_a}{RT} \quad (12)$$

where E is activation energy of reaction and A is frequency factor.

By using Coats-Redfern expression, the value of the activation energy (E_a) can be calculated from the slope of the plot of graph between ln[-ln(1-α)/T^2] and 1/T. The calculated activation energy is 92.33 KJ mol^{-1}.

Hirshfeld surface analysis: The property enhancement of the materials on the basis of crystal packing from various types of intermolecular contacts tends to molecular structural interpretation. The intermolecular interaction among the molecules, examined for single crystals for non-linear optical applications with the support of Hirshfeld surface and fingerprint plot. The knowledge of crystal packing, exclusively for the benefit of crystal design and crystal engineering. This assortment and summary will positively lead to a deeper assimilation of the intermolecular interaction and percentage contribution of each individual atom in the crystal lattice. In recent years interpretation of the molecular crystal structures using tools like Hirshfeld surfaces seem to be more significant. This concept reveals an approach to project the crystal packing diagrams, inter nuclear distances and angles, between the molecules depicted through distinct methods. In the formation of crystalline network, the intermolecular interactions [41,42] performs a pivotal role and hence analyzing that will enlighten the structure reliant crystalline properties [43]. Designing new crystal with appealing physical and chemical properties can be achieved by applying the knowledge gained from the intermolecular interactions existing in the framework of crystal packing [44]. Interpreting and managing the intermolecular forces like weak and strong hydrogen bonds, halogen-halogen interactions, π-π interactions, van der Waals forces, *etc*., plays a crucial role in crystal engineering effort [45]. Hirshfeld defined a weight function [46] for each atom in a molecule:

$$W_a(r) = \frac{\rho_a^{at}(r)}{\sum \rho_i^{at}(r)} \quad (13)$$

where the individual $\rho_i^{at}(r)$ are spherically averaged electron densities of the various atoms.

Hirshfeld surface analysis provides the visualization of intermolecular interactions in molecular crystals [47] and used to get the 3D Hirshfeld surfaces and 2D finger plots of the obtained crystal. By taking electron distribution as a sum of spherical atom electron densities, Hirshfeld surfaces are constructed [48]. The normalized contact distance d_{norm} based on the distance from a point on the surface to the nearest nucleus outside the surface, d_e is the distance from a point on the surface to the nearest nucleus inside the surface, d_i enables the identification of the regions of particular importance to the intermolecular interactions. The intermolecular contacts in the crystal lattice is provided by the combination of d_e and d_i in the form of two-dimensional fingerprint plot [49]. Hirshfeld surfaces mapped with d_{norm} and two dimensional fingerprint plots were generated by *CRYSTAL EXPLORER* 3.1 software program [50]. The normalized contact distance $d_{norm} = d_i - r_i^{vdw}/r_i^{vdw} + d_e - r_e^{vdw}/r_e^{vdw}$ where r_i^{vdw} and r_e^{vdw} are the van der Waals radii of the atoms. The intermolecular contact is shoreter than r^{vdw} if d_{norm} is negative and longer if d_{norm} is positive. The red-white-blue colour in Hirshfeld surface map represents the shortest intermolecular contact, contact around r^{vdw} separation and longer intermolecular contact distance respectively. The 2D fingerlpot is a combination of d_e and d_i provides the summary of intermolecular contacts in the crystal and are in complement to the Hirshfeld surfaces [51]. The shape index and curvedness are the two coloured properties can also be specified based on the

local curvature of the surface. The intermolecular interactions of the title compound are quantified using Hirshfeld surface analysis. Like Fourier transform infrared spectrum, Hirshfeld surfaces also unique for a particular crystal structure. The Hirshfeld surface analysis of *N*-acetylglycine was performed with the Crystal Explorer 3.1 program [50] using the experimental structure as input to reveal the inter molecular interactions in the crystal. Fig. 6 gives the complete finger print of the *N*-acetylglycine single crystal. Figs. 7 and 8 represent the 3D Hirshfeld surface (d_{norm}) and 2D fingerprint histogram of the molecule respectively. In Fig. 8, the red coloured points represent the intermolecular contacts shorter than the sum of their van der Waals radii (hydrogen bonds) while contacts greater than this sum are blue colour and white colours represent contacts around the sum of the van der Waals radii [52]. The d_{norm} values were determined to be in the range -0.1192 (negative points-red) to 1.2894 (positive points-blue) Å. In Fig. 7, C–H···O and C–H···N contacts are marked with green dashed lines with the C–H···O hydrogen bonds having a length of 2.443 Å and 2.916 Å, while the C-H···N hydrogen bonds have a length of 2.819 Å and 2.639 Å. The 2D fingerprint histograms shown in Fig. 7 indicate the contributions of the intermole-cular contacts to the Hirshfeld surfaces to be H···H (40.5%), N···H/H···N (1.4%), O···H/H···O (48.6%) and C···H/H···C (2.0%), respectively withincluded reciprocal interactions. The major contribution of inter-molecular contanct has been provided by H···H (40.5%) and O···H (48.6%).

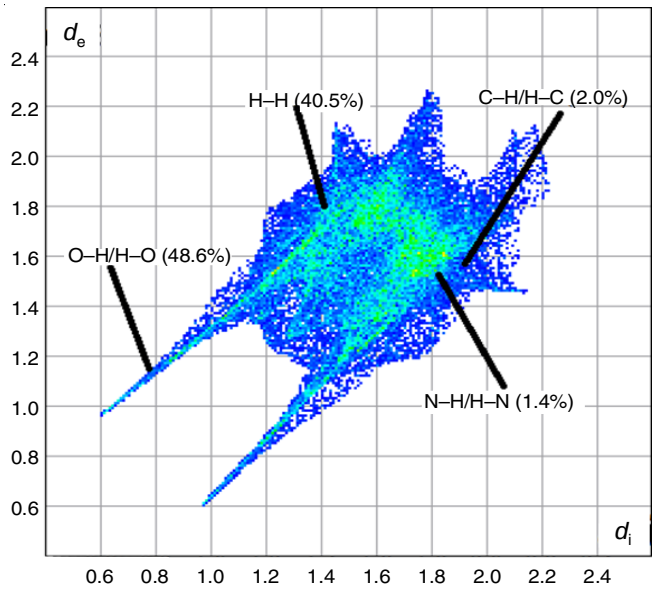

Fig. 6. Fingerprint of *N*-acetylglycine (100%)

Conclusion

N-Acetylglycine has been taken in the present study for hardness and thermal investigation. Hardness measurement study reveals that Vicker's hardness number (H_v) is varied for different loads. The work hardening coefficient value of 1.628 confirms that the grown crystal comes under moderately hard

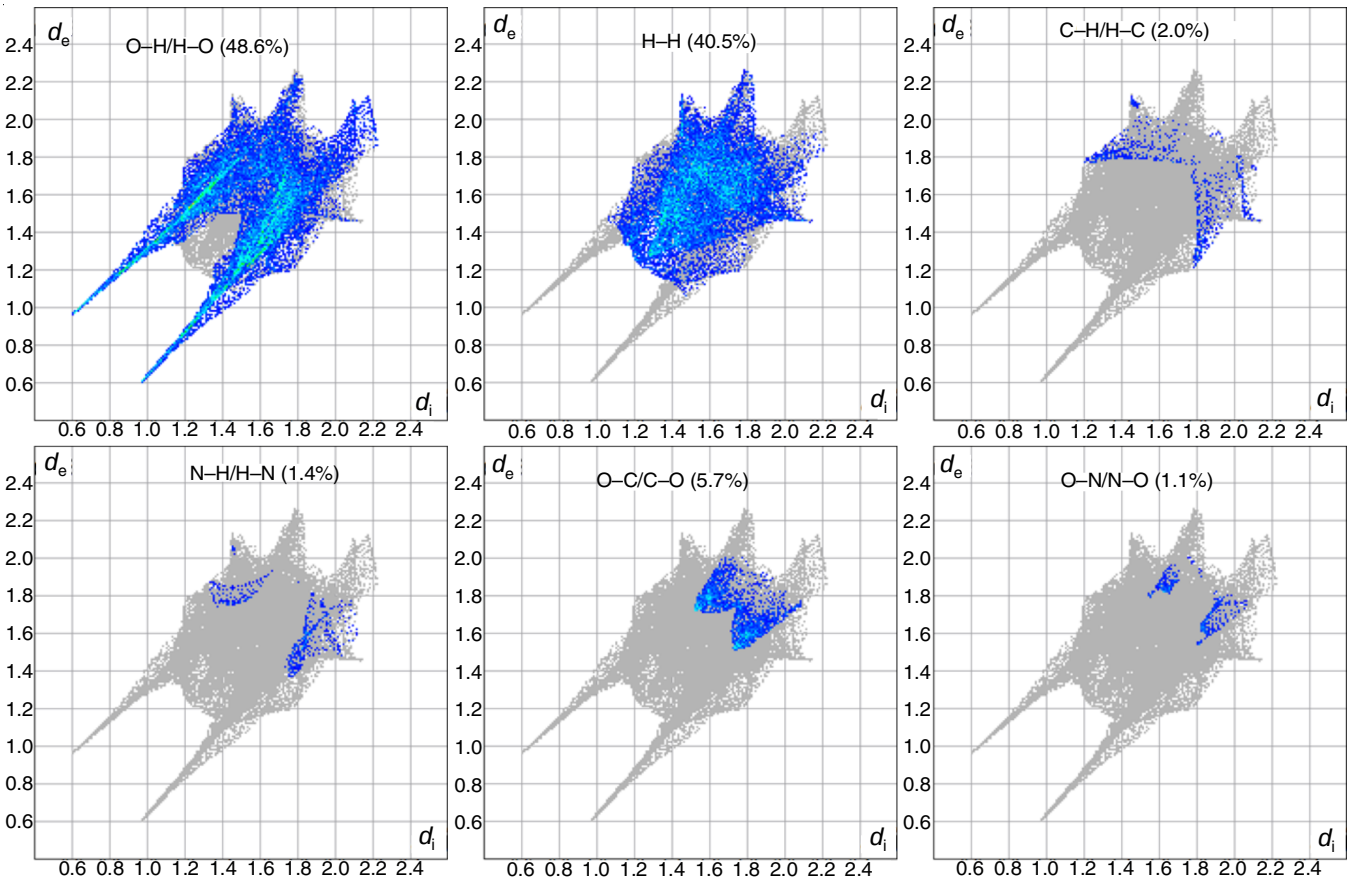

Fig. 7. Relative contributions to the percentage of Hirshfeld surface area for the various intermolecular contacts in *N*-acetylglycine

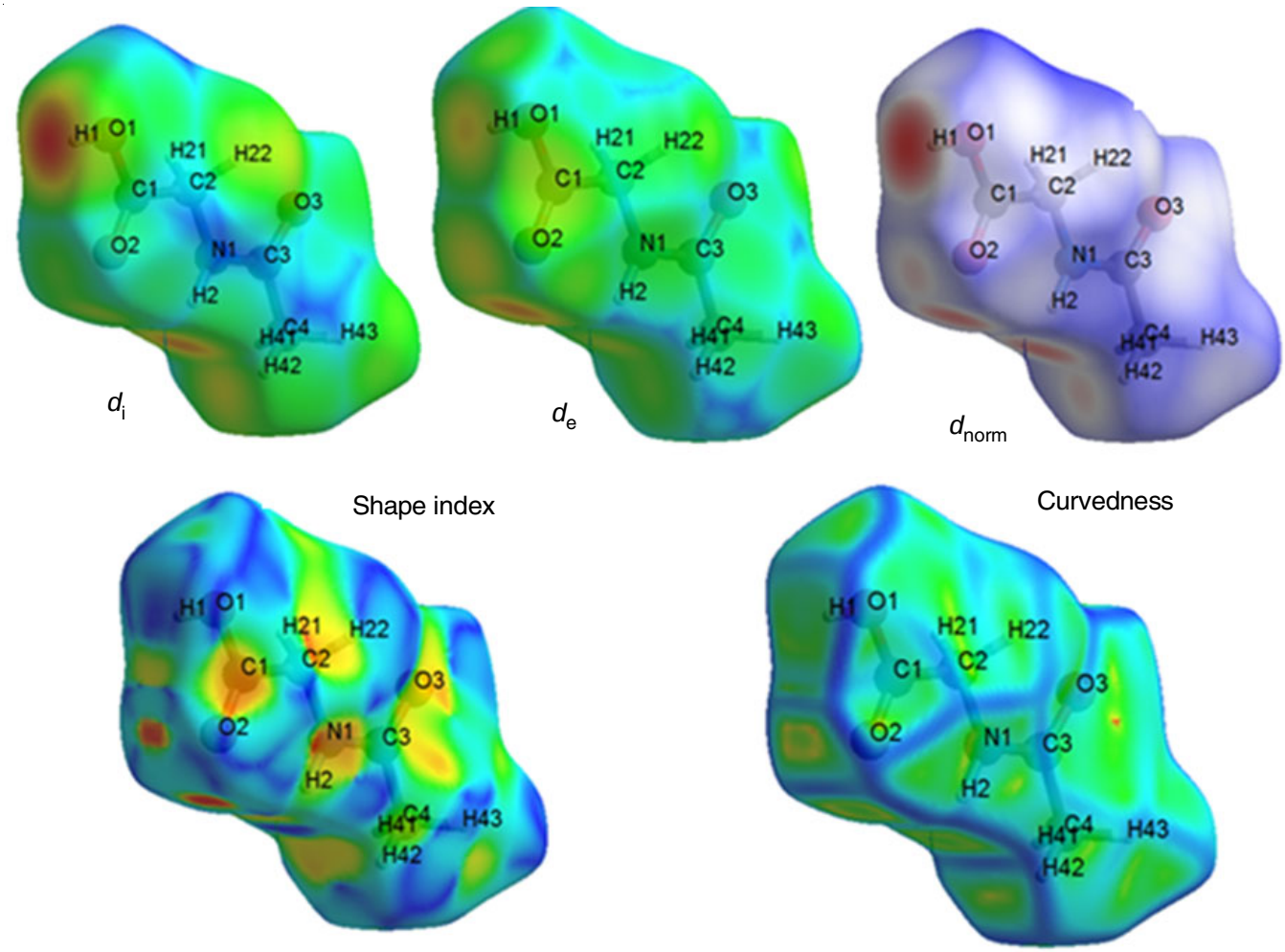

Fig. 8. Hirshfeld surface analysis d_i, d_e, d_{norm}, shape index and curvedness of *N*-acetylglycine

material category. The other mechanical parameters like minimum load indentation (W), materials constant (k_1), load dependent constant (A_1) and elastic stiffness constant (C_{11}) have also been calculated. The elastic stiffness coefficient of 2.346 gives the strength of the bond in *N*-acetylglycine crystal. The thermal analysis has also been carried and revealed that complete weight loss of *N*-acetylglycine starts from 208.60 ºC and ends at 281.58 ºC. The corresponding DTA peak is observed at 214.97 ºC which is the melting point of the sample. As expected, there is no phase transition till the material melts and this enhances the temperature range for the utility of crystal. Kinetic and thermodynamic parameters have been calculated. The activation energy is calculated by different single heating methods like Broido, Arrehenius, Horowitz-Metzger and Coats-Redfern method. The activation energy calculated by Arrehenius is found to be 122.04 KJ mol^{-1} which is higher than that of other methods. The entropy, enthalpy and Gibb's free energy of activation were estimated to be 197.73, 113.95 and 17.66 J K^{-1} mol^{-1}, respectively. All the results obtained from hardness as well as thermal measurement confirm the material may be suitable for pharmaceutical tableting and energetic material processing applications. The Hirshfeld surface analysis with finger plots and electrostatic potential map shed more light on the percentage of intermolecular contacts and distribution of electrostatic potential of *N*-acetylglycine compound. Also further research has to be carried out and can be extended to several industrial and research applications.

CONFLICT OF INTEREST

The authors declare that there is no conflict of interests regarding the publication of this article.

REFERENCES

1. M. Egart, B. Jankovic and S. Srèiè, *Acta Pharm.*, **66**, 303 (2016); https://doi.org/10.1515/acph-2016-0032
2. R.W. Armstrong and W.L. Elban, *Mater. Sci. Technol.*, **28**, 1060 (2012); https://doi.org/10.1179/1743284712Y.0000000012
3. J. Donohue and R.E. Marsh, *Acta Crystallogr.*, **15**, 941 (1962); https://doi.org/10.1107/S0365110X62002492
4. H. Etori, K. Taga, H. Okabayashi and K. Ohshima, *J. Chem. Soc., Faraday Trans.*, **93**, 313 (1997); https://doi.org/10.1039/a605741a
5. S. Bee, N. Choudhary, A. Gupta and P. Tandon, *Biopolymers*, **101**, 795 (2014); https://doi.org/10.1002/bip.22458
6. B. Boeckx and G. Maes, *J. Phys. Chem. A*, **116**, 1956 (2012); https://doi.org/10.1021/jp211382u
7. C. Bruyneel, A.K. Chandra, T. Uchimaru and T. Zeegers-Huyskens, *Spectrochim. Acta A Mol. Biomol. Spectrosc.*, **56**, 591 (2000); https://doi.org/10.1016/S1386-1425(99)00258-9

8. R.E. Vizhi, R.A. Kumar, D.R. Babu, K. Sathiyanarayanan and G. Bhagavannarayana, *Ferroelectrics*, **413**, 291 (2011); https://doi.org/10.1080/00150193.2011.531194)
9. J. Baran and A.M. Petrosyan, *Ferroelectrics*, **432**, 117 (2012); https://doi.org/10.1080/00150193.2012.707879
10. H. Kumar, M. Singla and H. Mittal, *J. Chem. Thermodyn.*, **94**, 204 (2016); https://doi.org/10.1016/j.jct.2015.10.017
11. D. Nagaraju, P.V. Raja Shekar, C.S. Chandra, K.K. Rao and N.G. Krishna, *AIP Conf. Proc.*, **1591**, 1259 (2014); https://doi.org/10.1063/1.4872923
12. T. Balakrishnan and K. Ramamurthi, *Mater. Lett.*, **62**, 65 (2008); https://doi.org/10.1016/j.matlet.2007.04.072
13. Y. Zhang, L. Feng and W. Qiu, *J. Mater. Sci.*, **54**, 9507 (2019); https://doi.org/10.1007/s10853-019-03543-3
14. N. Nithya, R. Mahalakshmi and S. Sagadevan, *Mater. Res.*, **18**, 581 (2015); https://doi.org/10.1590/1516-1439.007015
15. S. Suresh, A. Ramanand, P. Mani and K. Murthyanand, *J. Optoelectron Biomed. Mater.*, **1**, 129 (2010).
16. S. Sagadevan, *Int. J. Chem. Tech. Res.*, **6**, 2645 (2014).
17. A.A. Latha, M. Anbuchezhiyan, C.C. Kanakam and K. Selvarani, *Mater. Sci. Pol.*, **35**, 140 (2017); https://doi.org/10.1515/msp-2017-0031
18. S. Vyazovkin, A.K. Burnham, J.M. Criado, L.A. Pérez-Maqueda, C. Popescu and N. Sbirrazzuoli, *Thermochim. Acta*, **520**, 1 (2011); https://doi.org/10.1016/j.tca.2011.03.034
19. S. Vyazovkin and I. Dranca, *Macromol. Chem. Phys.*, **207**, 20 (2006); https://doi.org/10.1002/macp.200500419
20. V.L. Stanford, C.M. McCulley and S. Vyazovkin, *J. Phys. Chem. B*, **120**, 5703 (2016); https://doi.org/10.1021/acs.jpcb.6b03860
21. X.G. Li, M.R. Huang, G.-H. Guan and T. Sun, *Polym. Int.*, **46**, 289 (1998); https://doi.org/10.1002/(SICI)1097-0126(199808)46:4<289::AID-PI993>3.0.CO;2-O
22. X.G. Li, *J. Appl. Polym. Sci.*, **74**, 2016 (1999); https://doi.org/10.1002/(SICI)1097-4628(19991121)74:8<2016::AID-APP17>3.0.CO;2-T
23. N. Kanagathara, M.K. Marchewka, S. Gunasekaran and G. Anbalagan, *Acta Phys. Pol. A*, **126**, 827 (2014); https://doi.org/10.12693/APhysPolA.126.827
24. R. Bhuvaneswari, G. Vinitha and K. Sakthi Murugesan, *Appl. Phys., A Mater. Sci. Process.*, **125**, 385 (2019); https://doi.org/10.1007/s00339-019-2678-6
25. A. Bhaskaran, C.M. Ragavan, R. Sankar, R. Mohan Kumar and R. Jayavel, *Cryst. Res. Technol.*, **42**, 477 (2007); https://doi.org/10.1002/crat.200610851
26. K. Sangwal, *Cryst. Res. Technol.*, **44**, 1019 (2009); https://doi.org/10.1002/crat.200900385
27. M. Shkir, S. Muhammad, S. AlFaify, A. Irfan, M.A. Khan, A.G. Al-Sehemi, I.S. Yahia, B. Singh and I. Bdikin, *J. Saudi Chem. Soc.*, **22**, 352 (2018); https://doi.org/10.1016/j.jscs.2016.05.003
28. K. Boopathi, P. Rajesh, P. Ramasamy, Prapun Manyum, *Opt. Mater.*, **35**, 954 (2013); https://doi.org/10.1016/j.optmat.2012.11.015
29. T.B. Krishnan, P. Revathi, S. Sakthivel and K. Ramamurthi, *J. Taibah Univ. Sci.*, **12**, 208 (2018); https://doi.org/10.1080/16583655.2018.1451106
30. H. Kamari, N. Al-Hada, E. Saion, A. Shaari, Z. Talib, M. Flaifel and A. Ahmed, *Crystals*, **7**, 2 (2017); https://doi.org/10.3390/cryst7020002
31. K. Selvakumar, *Indian J. Sci. Technol.*, **9**, 1 (2016); https://doi.org/10.17485/ijst/2016/v9i36/101967
32. K. Harada, *Nature*, **214**, 479 (1967); https://doi.org/10.1038/214479a0
33. V.Y. Yablokov, I.L. Smel'tsova, I.A. Zelyaev and S.V. Mitrofanova, *Russ. J. Gen. Chem.*, **79**, 1704 (2009); https://doi.org/10.1134/S1070363209080209
34. A. Schaberg, R. Wroblowski and R. Goertz, *J. Phys. Conf. Ser.*, **1107**, 032013 (2018); https://doi.org/10.1088/1742-6596/1107/3/032013
35. N. Kanagathara, M.K. Marchewka, N. Sivakumar, N.G. Renganathan, K. Gayathri, S. Gunasekaran and G. Anbalagan, *J. Therm. Anal. Calorim.*, **112**, 1317 (2013); https://doi.org/10.1007/s10973-012-2713-8
36. K.J. Laidler, Chemical Kinetics, Harper & Row: New York (1987).
37. K.D. Parikh, D.J. Dave, B.B. Parekh, M.J. Joshi and Thermal, *Bull. Mater. Sci.*, **30**, 105 (2007); https://doi.org/10.1007/s12034-007-0019-4
38. A. Broido, *J. Polym. Sci. Part A-2*, **7**, 1761 (1969); https://doi.org/10.1002/pol.1969.160071012
39. H.H. Horowitz and G. Metzger, *Anal. Chem.*, **35**, 1464 (1963); https://doi.org/10.1021/ac60203a013
40. A.W. Coats and J.P. Redfern, *Nature*, **201**, 68 (1964); https://doi.org/10.1038/201068a0
41. S.L. Price, *J. Chem. Soc. Faraday Trans*., **92**, 2997 (1996); https://doi.org/10.1039/FT9969202997
42. S.L. Price, eds.: Ed.: A. Gavezzotti, Theoretical Aspects and Computer Modeling of the Molecular Solid State, Wiley: Chichester, pp. 31-60 (1997).
43. K.R. Seddon, eds.: K.R. Seddon and M. Zaworotko, Crystal Engineering, In: The Design and Application of Functional Solids, Kluwer Academic: Amsterdam, pp. 1-28 (1999).
44. F.H. Allen, *Acta Crystallogr. B*, **58**, 380 (2002); https://doi.org/10.1107/S0108768102003890
45. G.R. Desiraju, *Chem. Commun.*, 1475 (1997); https://doi.org/10.1039/a607149j
46. F.L. Hirshfeld, *Theor. Chim. Acta*, **44**, 129 (1977); https://doi.org/10.1007/BF00549096
47. M.J. Turner, J.J. McKinnon, S.K. Wolff, D.J. Grimwood, P.R. Spackman, D. Jayatilaka and M.A. Spackman, CrystalExplorer17 (2017).
48. M.A. Spackman, J.J. McKinnon and D. Jayatilaka, *CrystEngComm*, **10**, 377 (2008).
49. M.A. Spackman and J.J. McKinnon, *CrystEngComm*, **4**, 378 (2002); https://doi.org/10.1039/B203191B
50. S.K. Wolff, D.J. Greenwood, J.J. McKinnon, M.J. Turner, D. Jayatilaka and M.A. Spackman, Crystal Explorer, Version 3.1 (2012).
51. M.A. Spackman and J.J. McKinnon, *CrystEngComm*, **4**, 378 (2002); https://doi.org/10.1039/B203191B
52. M.A. Spackman and D. Jayatilaka, *CrystEngComm*, **11**, 19 (2009); https://doi.org/10.1039/B818330A